Histol Histopathol (2018) 33: 1059-1073

http://www.hh.um.es

Histology and Histopathology

From Cell Biology to Tissue Engineering

Identification of protein kinase C α- and tyrosine hydroxylase-immunoreactive cells in the microbat retina

Eun-Bee Park, Joo-Yeong Jeon and Chang-Jin Jeon

Department of Biology, School of Life Sciences, BK21 Plus KNU Creative BioResearch Group, College of Natural Sciences and Brain Science and Engineering Institute, Kyungpook National University, Daegu, South Korea

Summary. A growing number of studies have revealed the functional neuroarchitecture of the microbat retina and suggested that microbats can see using their eyes. To better understand the organization of the microbat retina, quantitative analysis of protein kinase C alpha (PKCα)- and tyrosine hydroxylase (TH)-immunoreactive (IR) cells was conducted on the greater horseshoe bat (*Rhinolophus ferrumequinum*) retina. As a result, PKCα immunoreactivity was observed in rod bipolar cells, consistent with previous studies on other mammalian retinas. PKCα-IR cell distribution in the inner nuclear layer showed regional differences in density, with the highest density found in the nasal retina. The average density of PKCα-IR cells was 10,487±441 cells/mm^2 (mean ± SD; n=4), with a total of 43,077±1,843 cells/retina. TH-IR cells in the *Rhinolophus ferrumequinum* retina could be classified into four types based on soma location and ramification in the inner plexiform layer: conventional amacrine, displaced amacrine, interplexiform, and intercalated cells. The majority of TH-IR cells were conventional amacrine cells. TH-IR cells were nonrandomly distributed at low density over the retina. The average density was 29.7±3.1 cells/mm^2 (mean ± SD; n=3), with a total of 124.0±11.3 cells/retina. TH-IR processes showed varicosities and formed ring-like structures encircling AII amacrine cells. Our study provides the foundation for understanding the neurochemical architecture of the microbat retina and supports the notion that the eyes do play a role in the visual system of microbats.

Key words: Microbat, Protein kinase C alpha, Tyrosine hydroxylase, Immunohistochemistry, Retina

Offprint requests to: Prof. Chang-Jin Jeon, Ph.D., Neuroscience Lab., Department of Biology, College of Natural Sciences, Kyungpook National University, 80 Daehakro, Bukgu, Daegu, 41566, South Korea. e-mail: cjjeon@knu.ac.kr

DOI: 10.14670/HH-18-001

Introduction

Rhinolophus ferrumequinum (*R. ferrumequinum*), the greater horseshoe bat, is a species of microbat characterized by a specific ecological niche that maintains darkness. Therefore, it has been recognized that microbats rely on echolocation, rather than visual ability, to find prey, recognize their surroundings, and navigate (Jones and Rayner, 1989; Altringham, 2011). However, microbats were reported to have functional eyes capable of ultraviolet and scotopic vision (Eklöf, 2003; Winter et al., 2003; Müller et al., 2009; Orbach and Fenton, 2010), and recent studies on the localization of neuronal cells containing various neurotransmitters and their visual organization in the microbat retina support the possibilities of photic and scotopic vision (Studholme et al., 1987; Jeon et al., 2007; Kim et al., 2008; Feller et al., 2009; Müller et al., 2009, 2013; Butz et al., 2015; Park et al., 2017). Although many studies have focused on the microbat retina, the retinal neuronal cytoarchitecture and visual abilities of microbat are not yet fully understood.

The retina is composed of more than sixty cellular subtypes classified by their distinctive morphologies, locations, and functions. For instance, depending on the

animal species, cone bipolar, amacrine, and ganglion cells consist of 10-15, 30-40, and 25-30 subtypes, respectively (Masland, 2004; Euler et al., 2014; Butz et al., 2015; Sanes and Masland, 2015; Baden et al., 2016). However, rod bipolar cells are classified into only one type, and their morphology is similar in many mammalian retinas. Since protein kinase C alpha (PKCα) is expressed by rod bipolar cells in most mammalian retinas, PKCα is an established marker for rod bipolar cells (Negishi et al., 1988; Greferath et al., 1990; Zhang and Yeh, 1991; Young and Vaney, 1991; Strettoi and Masland, 1995; Casini et al., 1996; Caminos et al., 2000). The physiological role of PKCα in rod bipolar cells is not yet fully understood, but it is involved in cytoplasmic Ca^{2+}-dependent signaling pathways, proliferation, differentiation, regulation of dopamine release in the central nervous system, and modulation of temporal properties of the light response in the rod visual pathway (Nishizuka, 1988, 1992; Conn and Sweatt, 1994). Rod bipolar cells make synaptic connections with ganglion cells via amacrine cells, including the AII amacrine cells (Wässle et al., 1995); therefore, studies on rod bipolar cells are considerably important.

AII amacrine cells also receive synaptic inputs from dopaminergic amacrine cells (Voigt and Wässle, 1987). Several studies have shown that dopamine regulates the permeability of gap junctions between AII amacrine cells, and that the processes of dopaminergic neurons are in close apposition to the soma of AII amacrine cells forming ring-like structures around them (Voigt and Wässle, 1987; Dacey, 1990). Tyrosine hydroxylase (TH), a rate-limiting enzyme for dopamine biosynthesis, has been used as a marker in identifying dopaminergic cells, due to its specific labeling (Versaux-Botteri et al., 1984, 1986; Oyster et al., 1985; Mitrofanis et al., 1988; Dacey, 1990; Eglen et al., 2003). Previous studies have described the characteristics of TH-immunoreactive (IR) dopaminergic neurons in the retina, such as low densities, wide-field processes, varicosities, and ring-like structures. There are, however, species differences in the types of TH-IR cells (Dowling, 1987; Dacey, 1990; Rodieck, 1998). According to previous studies, TH-IR cells in mammalian retinas are generally classified into one to three types based on their cellular morphology (Brecha et al., 1984; Versaux-Botteri et al., 1984; Oyster et al., 1985; Versaux-Botteri et al., 1986; Mitrofanis et al., 1988; Zhu and Straznicky, 1990; Guimarães and Hokoç, 1997; Kicliter et al., 1999).

Previously, we showed the presence of AII amacrine cells in the *R. ferrumequinum* retina by specific labeling with parvalbumin antibody (Jeon et al., 2007) and reported their spatial density and distribution pattern. We also identified and described the distribution of photoreceptors (Kim et al., 2008) and cholinergic amacrine cells (Park et al., 2017) in the same species. Our previous studies provided some basic information on the neuronal cytoarchitecture of the microbat retina, and supported the possible view of having a functional neurocircuitry for vision in the *R. ferrumequinum* retina. Although the presence of TH- and PKCα-IR cells in the microbats has been reported previously (Studholme et al., 1987; Müller et al., 2013; Butz et al., 2015), the quantitative analysis of these cells in the microbat retina has not yet been conducted. In the present study, we present a quantitative analysis such as spatial density and distributional pattern of PKCα-IR rod bipolar cells and TH-IR dopaminergic cells, two important elements that connect to AII amacrine cells in the microbat retina. The data will contribute to a better understanding of bat visual systems by providing information on the neuronal cytoarchitecture of the retina related to the visual ability of microbats, and clues to comprehend the functional role of the microbat retina.

Materials and methods

Animals and tissue preparation

Adult microbats (*R. ferrumequinum*, N=11, both sexes: 15-20 g) used in this study were caught in a cave in the districts of Miryang and Gimcheon, South Korea. After 2-3 h of transportation, the bats were anesthetized with a mixture of zoletil (10-25 mg/kg) and xylazine (3-6 mg/kg) before perfusion. Following a pre-rinse with phosphate-buffered saline (PBS, pH 7.4) for 3-5 min, each bat was perfused with 30-50 ml of fixative for 20-30 min via a syringe needle inserted into the left ventricle and aorta. They were perfused intracardially with 4% paraformaldehyde and 0.3-0.5% glutaraldehyde in 0.1 M sodium phosphate buffer (PB, pH 7.4) containing 0.002% calcium chloride. The eyes were then enucleated, and the anterior segment of the eye, including the vitreous body and lens, was removed. Retinas were post-fixed with 4% paraformaldehyde in 0.1 M PB (pH 7.4) for 2 h at 4°C. Experiments were carried out in accordance with the Association for Research in Vision and Ophthalmology (ARVO) guidelines, and the National Institutes of Health (NIH) guidelines for the use of animals. All animal experiments were approved by the Institutional Animal Care and Use Committee of Kyungpook National University (permission no. 2016-0151) and in compliance with the Korean laws of Natural Protection. All efforts were made to minimize animal suffering and number of animals used.

Immunohistochemistry

After being rinsed 3×10 min in 0.1 M PB, fixed retinas were processed as whole mount retinas or 50 μm-thick vertical sections obtained with a Vibratome 3000 Plus Sectioning System (Vibratome, St. Louis, MO, USA). Monoclonal antibody against PKCα (mouse anti-PKCα, 1:200; Amersham Life Science, Buckinghamshire, England) and polyclonal antibody against TH (rabbit anti-TH, 1:200; Pel-Freez, Rogers, AR, USA) were the primary antibodies used. Additionally,

monoclonal antibody against parvalbumin (mouse anti-PV, 1:500) obtained from Sigma-Aldrich (St. Louis, MO, USA) was used as an AII amacrine cell marker (Gábriel and Straznicky, 1992; Wässle et al., 1993; Casini et al., 1995; Jeon et al., 2007). For primary antibody detection by immunofluorescence, the secondary antibodies used were fluorescein isothiocyanate (FITC)-conjugated horse anti-mouse/goat anti-rabbit IgG (1:100; Vector Laboratories, Burlingame, CA, USA), Texas red-conjugated horse anti-mouse (1:200; Vector Laboratories), and biotinylated goat anti-rabbit IgG (1:200; Vector Laboratories). Fluorescence and horseradish peroxidase (HRP) immunohistochemical methods have been previously described in detail (Jeon and Jeon, 1998). To identify the retinal layers, nuclei of the retina were stained with DAPI (1:1000; SouthernBiotech, Birmingham, AL, USA) or ethidium homodimer (1:1000; Molecular Probes, Eugene, OR, USA). Following immunohistochemistry procedures, the tissues were mounted on glass slides with Vectashield mounting medium (Vector Laboratories) and covered with a coverslip. Cells were imaged with a laser scanning confocal microscope (MRC 1024; Bio-Rad, Hercules, CA, USA) equipped with a 20× objective (NA 0.50, Plan Fluor; Nikon, Tokyo, Japan) and a 40× objective (NA 0.75, Plan Fluor; Nikon), then photographed with a Zeiss Axioplan microscope containing conventional or differential interference contrast (DIC) optics (Carl Zeiss, Jena, Germany).

To confirm the specificity of the primary rabbit anti-TH antibody, negative control and preabsorption tests were conducted on the bat retina. For the negative control test, the immunohistochemistry protocol remained the same, except for the primary antibody, which was excluded. For the preabsorption test, recombinant TH (Biomatik, Wilmington, DE, USA) was mixed with the primary antibody at a ratio of 10:1 to inactivate the primary antibody. After 1 h of pre-incubation of the mixture at room temperature, retinal tissues were incubated with the preabsorbed antibody in place of the primary antibody. Bat retinal tissues showed no TH immunoreactivity in negative control and preabsorption tests.

Data analysis

Whole mount retinas of *R. ferrumequinum* were quantitatively analyzed for cell density. In three whole mount retinas, PKCα-IR cells in the inner nuclear layer (INL) were imaged on a monitor using a 20× objective (Plan-Apochromat; Carl Zeiss) and an AxioCam HRc digital camera (Carl Zeiss) at 200 μm intervals along the

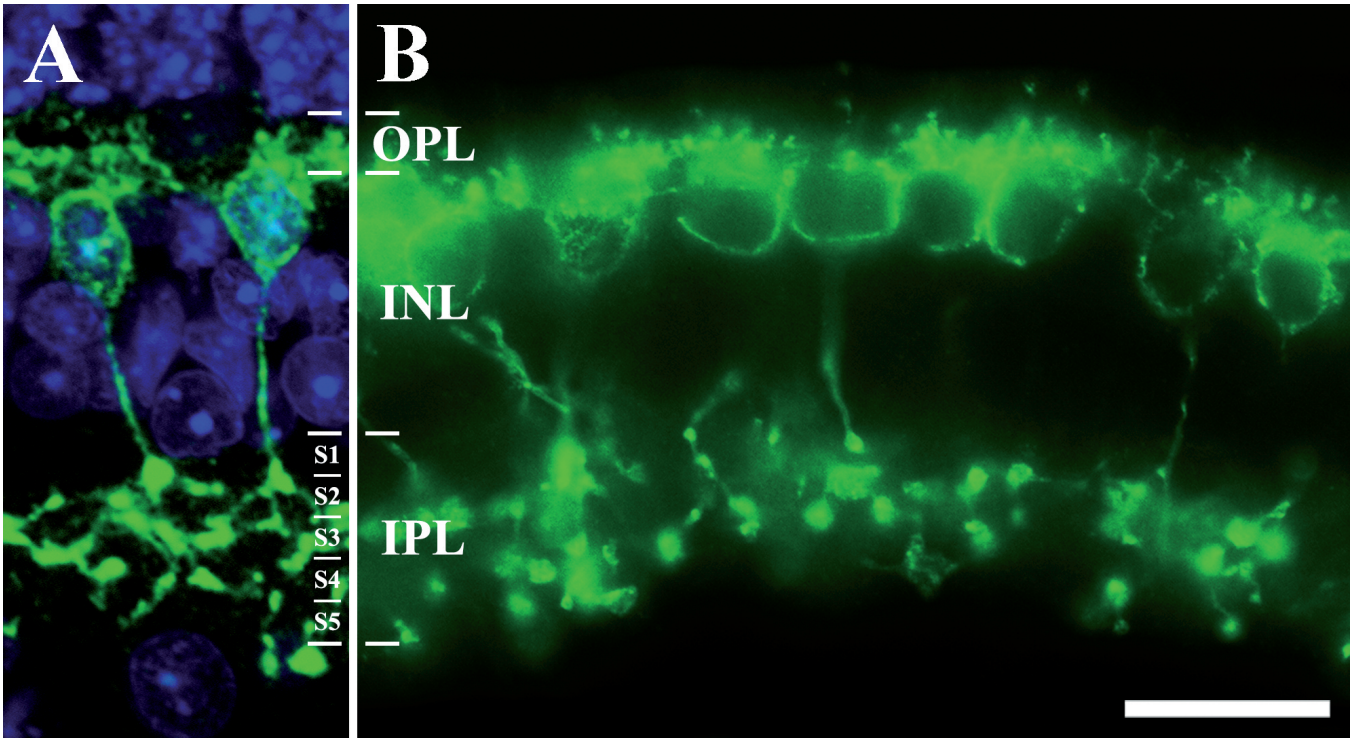

Fig. 1. PKCα *R. ferrumequinum* retinas. **A.** PKCα immunoreactivity (green) with DAPI staining (blue) to easily visualize the localization of PKCα-IR cells and their processes in the retinal layers. **B.** Somata of PKCα-IR cells are visible in the outermost part of the INL, and their axon terminals extend to the lower IPL showing the characteristic appendages. Characteristic axonal swellings are visible in the middle (S3) and lower IPL (S4, S5). Branched dendritic processes are also visible in the OPL. OPL, outer plexiform layer; INL, inner nuclear layer; IPL, inner plexiform layer; S, sublamina. Scale bar: 20 μm.

central dorsoventral and nasotemporal axes. Sample areas (37-39 per retina) of 100×100 μm^2 were taken at evenly distributed positions across the retina. To count the PKCα-IR cells, a transparent sheet was placed on the computer monitor and labeled cells were circled with a pen. PKCα-IR cells were counted and analyzed in a total number of 115 sample areas across the whole mount retinas. In one whole mount retina, total PKCα-IR cells were counted to draw an isodensity map of the cell distribution. Isodensity contours were made to fit the data using a gray scale indicating regions of highest density as black and increasingly lighter gray for areas of decreasing density. The total number of cells was determined in each sample area and cell density was expressed as the number of cells per square millimeter. Cell density was then multiplied by retinal area to determine the total number of PKCα-IR cells. Retinal area could be measured using the Automeasure® function of AxioVision program (Carl Zeiss), which automatically measures the area when marked along the rim of the retina. TH-IR cells in three whole mount retinas were quantitatively analyzed for their cell density as described for PKCα-IR cells. TH-IR cells were counted in three whole retinas by dividing them into cells located in the INL and ganglion cell layer (GCL).

A nearest-neighbor analysis was performed on the TH-IR cells located in the INL of whole mount retinas. The nearest-neighbor analytical method to determine the regularity index was performed as previously described (Wässle and Riemann, 1978; Wässle et al., 1993; Cook, 1996). The regularity indexes were determined by dividing mean nearest-neighbor distances by their respective standard deviations.

Results

PKCα-IR cells in R. ferrumequinum retina

Figure 1 shows PKCα immunoreactivity in a 50-μm vertical section of the bat retina. Somata of the PKCα-IR cells were observed in the outermost part of the INL, and their dense plexus of axonal terminal arborizations extended to the lower inner plexiform layer (IPL) showing the characteristic appendages. Their axonal swellings were visible in the lower IPL (sublaminae S4 and S5; Fig. 1) and also in the middle IPL (sublamina S3; Fig. 1). Branched dendritic processes were also visible in the outer plexiform layer (OPL). Morphology of the PKCα-IR cells in the whole mount bat retina was

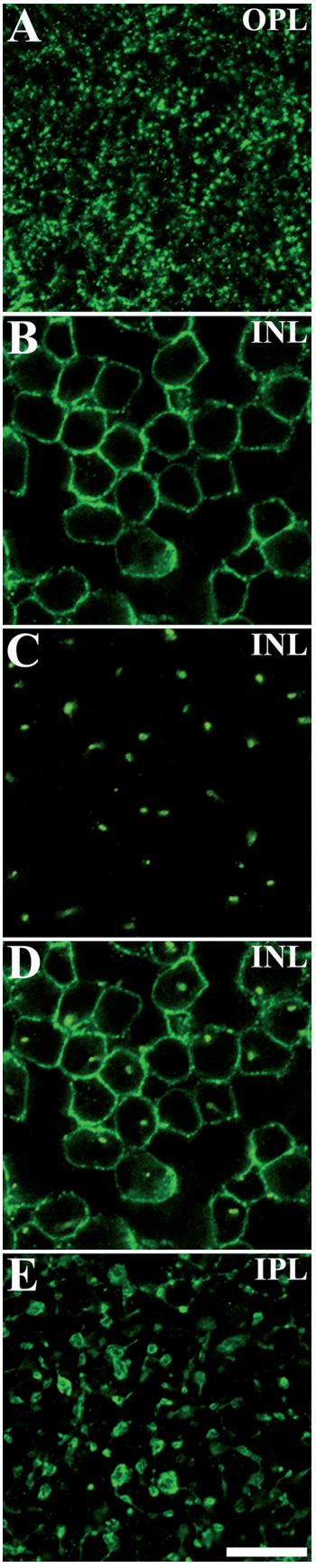

Fig. 2. PKCα-IR cells in a whole mount *R. ferrumequinum* retina. **A.** Dendritic processes spread out over the OPL. **B.** PKCα immunoreactivity observed on the membrane of somata in the outer INL. **C.** Axons of PKCα-IR cells. **D.** Superimposed image of **(B)** and **(C)** showing that axons and somat locations coincide. **E.** PKCα-IR axon terminals in the inner IPL, showing the characteristic appendages. OPL, outer plexiform layer; INL, inner nuclear layer; IPL, inner plexiform layer. Scale bar: 20 μm.

imaged using a high-magnification confocal microscope (Fig. 2). PKCα-IR dendritic processes were visualized in the OPL of the bat retina (Fig. 2A) and PKCα immunoreactivity was evident on the membrane of the somata in the outermost part of the INL (Fig. 2B). Axons of the PKCα-IR cells were observed within the INL and extended towards the IPL (Fig. 2C). The locations of axons and somata were coincident, as revealed in a superimposed image (Fig. 2D). PKCα-IR axonal terminals in the IPL have the characteristic appendages of rod bipolar cell axon terminals (Fig. 2E). These morphological characteristics of PKCα immunoreactivity in the *R. ferrumequinum* retina were typical of rod bipolar cells.

Distribution of PKCα-IR cells in R. ferrumequinum retina

The estimated total numbers of PKCα-IR cells in the bat retina varied from 40,561 to 44,732 cells among the four retinas sampled. The average number of PKCα-IR cells per retina was 43,077±1,843 (mean ± S.D.; n=4), and the mean density was 10,487±441 cells/mm^2 (n=4; Table 1). Distribution of total PKCα-IR cells is shown in Fig. 3, with the cell density represented in a retinal isodensity map whose lines encircle higher density areas (Fig. 3A). The retinal map revealed regional differences in cell density distribution of PKCα-IR cells in the INL, with the highest density area being the mid-central region of the nasal retina. Based on the number of PKCα-IR cells encountered along the dorsoventral and nasotemporal axes intersecting the optic nerve head, the peak density (14,900 cells/mm^2, n=4) appeared in the mid-central nasal retina approximately 200 μm away from the optic nerve head (Fig. 3B,C). PKCα-IR cell density was lower in the marginal regions of the retina and was lowest (4,800 cells/mm^2, n=4) in the peripheral region of the temporal retina (Fig. 3B,C). The nasotemporal curve (Fig. 3C) displayed an asymmetric distribution, while the dorsoventral curve (Fig. 3B) displayed an almost symmetrical distribution of PKCα-IR cells in the INL.

TH-IR cells in R. ferrumequinum retina

Somata of amacrine cells and their processes in *R. ferrumequinum* retinas were strongly labeled with anti-TH antibodies. TH-IR cells were classified into four types of retinal cells, including two major types - conventional amacrine cells (Fig. 4A-C) and displaced amacrine cells (Fig. 4D-F) - and two minor types - interplexiform cells (Fig. 4G, H) and intercalated cells (Fig. 4I) - based on somata location and dendritic ramification within the INL. Most TH-IR cells possessed medium- to large-size somata in the innermost border of the INL, and their processes extended horizontally in the IPL (Fig. 4A,B). The somata of conventional amacrine cells were located in the INL (Fig. 4A-C) and the somata of displaced amacrine cells were located in the GCL (Fig. 4D-F). However, the ramification of TH-IR displaced amacrine cells (Fig. 4D-F) was similar to TH-IR conventional amacrine cells (Fig. 4A-C). All TH-IR conventional amacrine cells in the bat retina extended

Table 1. Total protein kinase C alpha-immunoreactive cells in the *R. ferrumequinum* retina.

Retina	Total analyzed area* (μm^2)	Cells counted	Total retinal area (μm^2)	Mean density (cells/mm^2)	Total PKCα-IR cells
Retina #1R	370,000	3,958	4,124,535	10,697	44,120
Retina #2L	390,000	4,254	4,101,201	10,907	42,894
Retina #3R	390,000	4,079	4,101,231	10,458	44,732
Retina #4R	4,103,254	40,561	4,103,254	9,885	40,561
Mean ± SD				10,487±441	43,077±1,843

PKCα, protein kinase C alpha; IR, immunoreactive; R, right; L, left; SD, standard deviation. * One sampled area (sampled in retinas #1R, #2L and #3R)= 100×100 μm^2.

Table 2. Total tyrosine hydroxylase-immunoreactive cells in the *R. ferrumequinum* retina.

Retina	Total retinal area (μm^2)	Neurons counted				Total TH-IR cells counted (cells/retina)	Mean density (cells/mm^2)
		Soma in INL		Soma in GCL			
		Counted	Mean density (cells/mm^2)	Counted	Mean density (cells/mm^2)		
Retina #1L	4,402,916	109	24.8	9	2	118	26.8
Retina #2R	4,145,976	129	31.1	8	1.9	137	33
Retina #3L	3,991,025	105	26.3	12	3	117	29.3
Mean ± SD		114.3±12.9	27.4±3.3	9.7±2.1	2.3±0.6	124.0±11.3	29.7±3.1

TH, tyrosine hydroxylase; IR, immunoreactive; INL, inner nuclear layer; GCL, ganglion cell layer; L, left; R, right; SD, standard deviation.

their processes horizontally in the outermost border of the IPL (Fig. 4A-C). TH-IR conventional amacrine cells (n=212 analyzed) had mostly monostratified processes (Fig. 4A; n=105), but other subtypes possessed bistratified (Fig. 4B; n=83) or multistratified processes (Fig. 4C; n=24). TH-IR displaced amacrine cells (n=22 analyzed) also had processes that extended horizontally in the outermost border of the IPL (Fig. 4D; n=11), and some subtypes had bistratified (Fig. 4F; n=8) or multistratified processes (Fig. 4E; n=3). In both TH-IR types, multistratified processes (approximately 10%) were observed less frequently than monostratified (approximately 50%) or bistratified processes (approximately 40%). Interplexiform cells with processes extending towards the OPL (arrows in Fig. 4G, H) were observed in the *R. ferrumequinum* retina. Some TH-IR fibers from the IPL extended through the INL to the OPL (Fig. 4H). Moreover, intercalated TH-IR somata were observed in the middle of the IPL (Fig. 4I). These cells rarely appeared, with only 1-2 cells in the whole retina, extending their processes in the middle of the IPL. Soma size of the intercalated TH-IR cells was the same size as the soma of the conventional amacrine cells.

Figure 5 shows the overall distribution and the dense plexus of TH-IR cells in whole mount bat retina. Figure 5A was taken from the peripheral region of the bat retina and shows the distribution of TH-IR conventional and displaced (arrowheads) amacrine cells. TH-IR cells typically had 2-5 primary processes, derived from the soma, that extended radially forming a large branched field in the bat retina. Therefore, the TH-IR processes extensively overlapped with each other and considerably covered the retina (Fig. 5A). Varicosities of TH-IR amacrine cell processes and ring-like structures formed by some varicose processes were visible (asterisks in Fig. 5B,C). In a superimposed image (Fig. 5E) ring-like structures of TH-IR processes (asterisks in Fig. 5C) and AII amacrine cells (Fig. 5D) labeled with parvalbumin antibody (Jeon et al., 2007) were observed together. The majority of the somata (70%) of AII amacrine cells located in the INL were encircled by TH-IR processes. The characteristic ring-like structures encircling the AII amacrine cells in the bat retina were clearly evident at a higher magnification (Fig. 5F-I) of the square regions marked in figure 5E.

Distribution of TH-IR cells in R. ferrumequinum retina

TH-IR cells in the INL and the GCL were counted in three whole mount retinas. The estimated total number of TH-IR cells in the INL of the three retinas varied from 105 to 129 cells, with a mean cell number and density of 114.3±12.9 cells and 27.4±3.3 cells/mm^2, respectively (Table 2). The estimated total number of TH-IR cells in the GCL varied from 8 to 12 cells (9.7±2.1 cells), with a mean density of 2.3±0.6 cells/mm^2 (Table 2). In the bat retina, the total number of TH-IR cells ranged from 117 to 137 cells (124.0±11.3 cells), and the mean density of

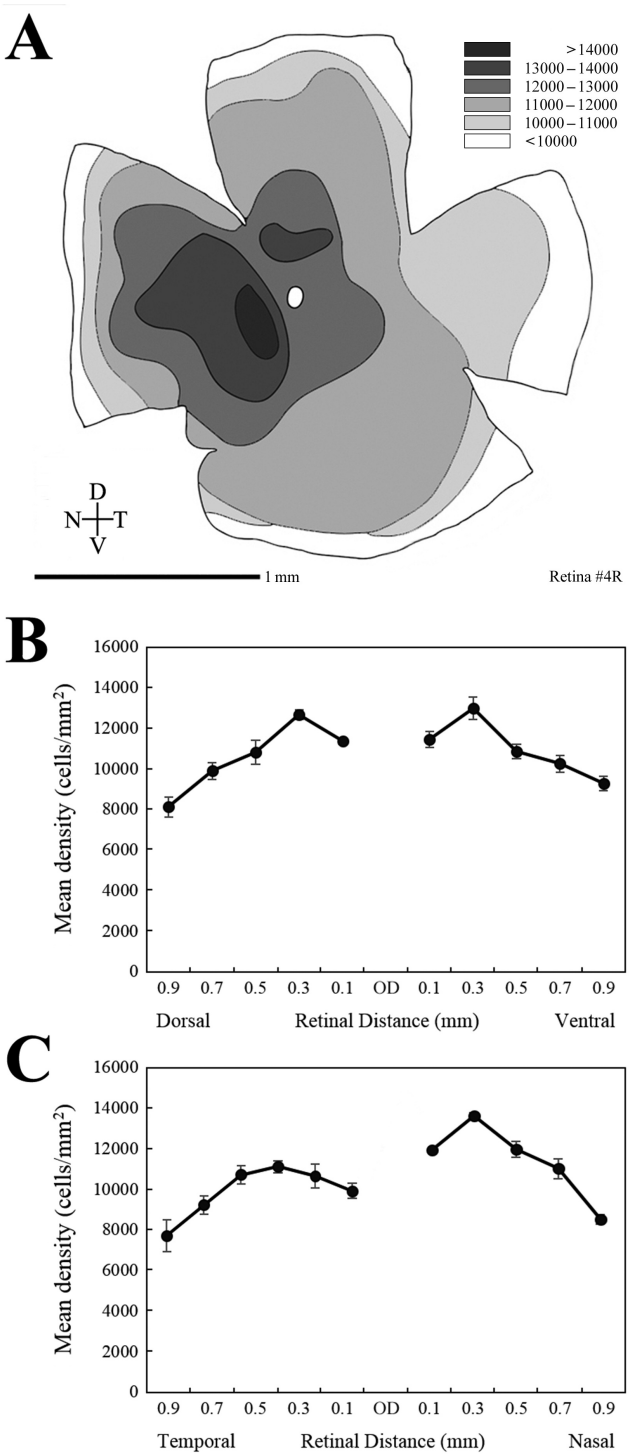

Fig. 3. PKCα-IR cells in the INL of *R. ferrumequinum* retinas. **A.** Isodensity map of the distribution of PKCα-IR cells reconstructed from whole mount fluorescence immunohistochemistry. The map includes isodensity lines, and the density values are given as cells/mm^2. **B, C.** Number of PKCα-IR cells encountered along the two axes (B, dorsoventral; C, nasotemporal) intersecting at the optic nerve head was expressed as mean density in the four retinas with standard deviation. D, dorsal; N, nasal; V, ventral; T, temporal parts; R, right; OD, optic disc.

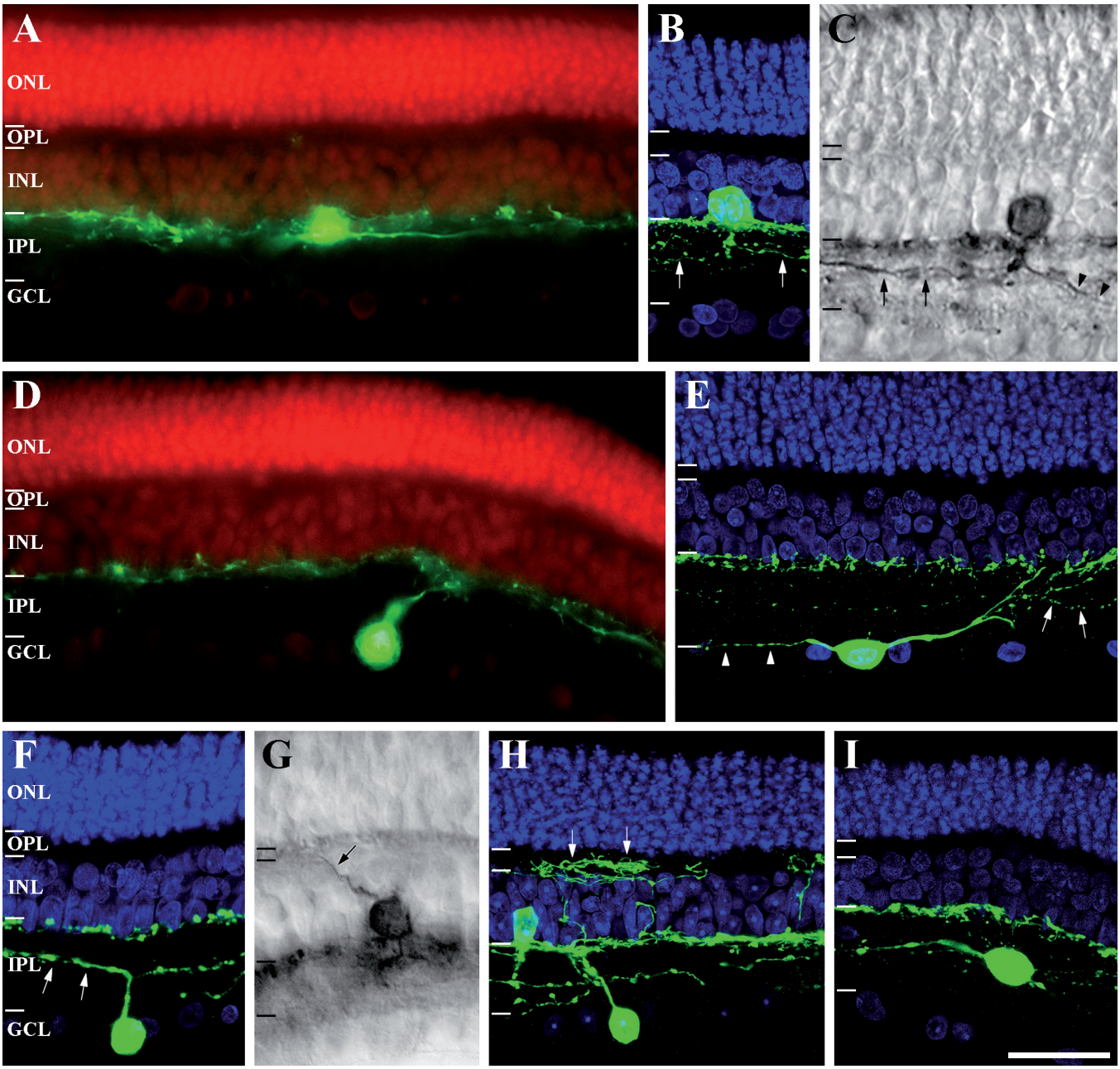

Fig. 4. TH-IR cells in the *R. ferrumequinum* retina. **A, D.** Fluorescence micrographs of the ethidium-homodimer-stained (red) vertical sections showing TH immunoreactivity (green). **B, E, F, H, I.** Fluorescence micrographs of the DAPI-stained (blue) vertical sections showing TH immunoreactivity (green). **C, G.** Differential interference contrast micrographs of the vertical sections showing HRP-stained TH immunoreactivity. **A-C.** Conventional amacrine cells with **(A)** monostratified processes at the outermost IPL, **(B)** bistratified in the outermost and middle IPL (arrows), and **(C)** a multistratified branch to the innermost IPL (arrowheads). Somata of TH-IR conventional amacrine cells are located in the innermost border of the INL, and their processes extend horizontally, mainly in the outermost IPL, with additional occasional stratification (arrows and arrowheads). **D-F.** Displaced amacrine cells. Somata of TH-IR displaced amacrine cells are located in the GCL and ramification is similar to that of the TH-IR conventional amacrine cells. **D.** Their processes mainly extend to the outermost IPL, **(E, F)** occasionally to the middle of the IPL (arrows in **E**, **F**), and are rarely multistratified (arrowheads in **E**). **G.** An interplexiform cell with a thin process (arrow) from the soma of the TH-IR cell extending to the OPL. **H.** Some TH-IR fibers (arrows) extending to the OPL. **I.** An intercalated TH-IR cell. Soma of a rarely observed intercalated TH-IR cell located in the middle of the IPL, with processes also extending to the middle of the IPL. ONL, outer nuclear layer; OPL, outer plexiform layer; INL, inner nuclear layer; IPL, inner plexiform layer; GCL, ganglion cell layer. Scale bar: 20 μm.

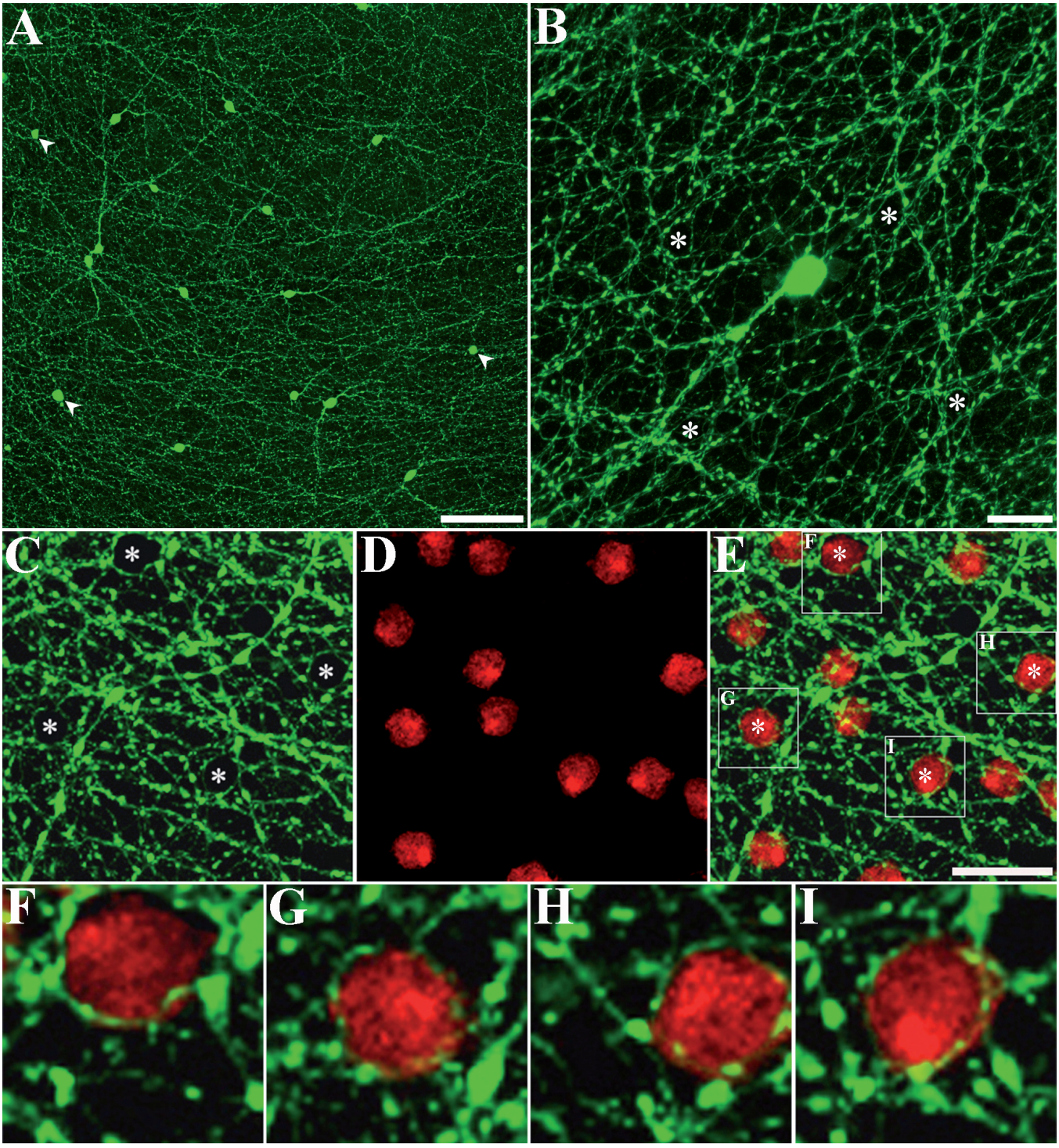

Fig. 5 TH-IR cells in the whole mount retina of *R. ferrumequinum*. **A.** Low magnification confocal image showing the distribution of TH-IR cells in the peripheral region of the bat retina. Arrowheads indicate TH-IR displaced amacrine cells. The others are TH-IR conventional amacrine cells. **B.** Higher magnification confocal image showing a TH-IR conventional amacrine cell. TH immunoreactivity is found within the cytoplasm and processes emanating from the somata. Varicosities of the TH-IR processes are visible, with asterisks indicating the ring-like structures. **C-I.** Projection of 8 scans of a *R. ferrumequinum* retina section showing colocalization of TH-IR cells and AII amacrine cells. **C.** TH-IR processes located in the IPL showing varicosities. Ring-like structures indicated with asterisks are shown in the higher magnification panels. **D.** Somata of AII amacrine cells labeled with parvalbumin antibody. **E.** Superimposed image of **(C)** and **(D)**. Parvalbumin-IR cells (red) are encircled by TH-IR dendritic rings (green). **F-I.** Magnified images of the square regions marked in **(E)**, showing the morphological relationship between the TH-IR ring-like structures and somata of AII amacrine cells. Scale bar: A, 100 µm; B, E, 20 µm.

total TH-IR cells was 29.7±3.1 cells/mm^2 (Table 2). Approximately 92% of the total TH-IR cells were distributed in the INL with only 8% in the GCL. This distribution was visualized in whole retinal maps (Fig. 6A,C,E). In the GCL, the somata of the TH-IR cells were distributed irregularly and were preferentially located in the peripheral region of the retina.

The retinal mosaic of TH-IR cells in the INL was visualized in histograms using nearest-neighbor analysis (Wässle and Riemann, 1978). The nearest-neighbor distance of TH-IR somata located in the INL of three different whole mount retinas ranged from 114.95 to 154.15 μm (137.48±20.25). The regularity index of TH-IR conventional amacrine cells was 2.14±0.05, ranged from 2.09 to 2.17 (Fig. 6B,D,F). TH-IR cells in the GCL were not used for nearest-neighbor analysis as the distribution of these cells was irregular.

Discussion

Morphology of PKCα-IR cells in R. ferrumequinum retina

PKCα is a common marker used to morphologically distinguish rod bipolar cells in vertebrate retinas (Negishi et al., 1988; Greferath et al., 1990; Kolb et al., 1993; Casini et al., 1996; Kosaka et al., 1998; Caminos

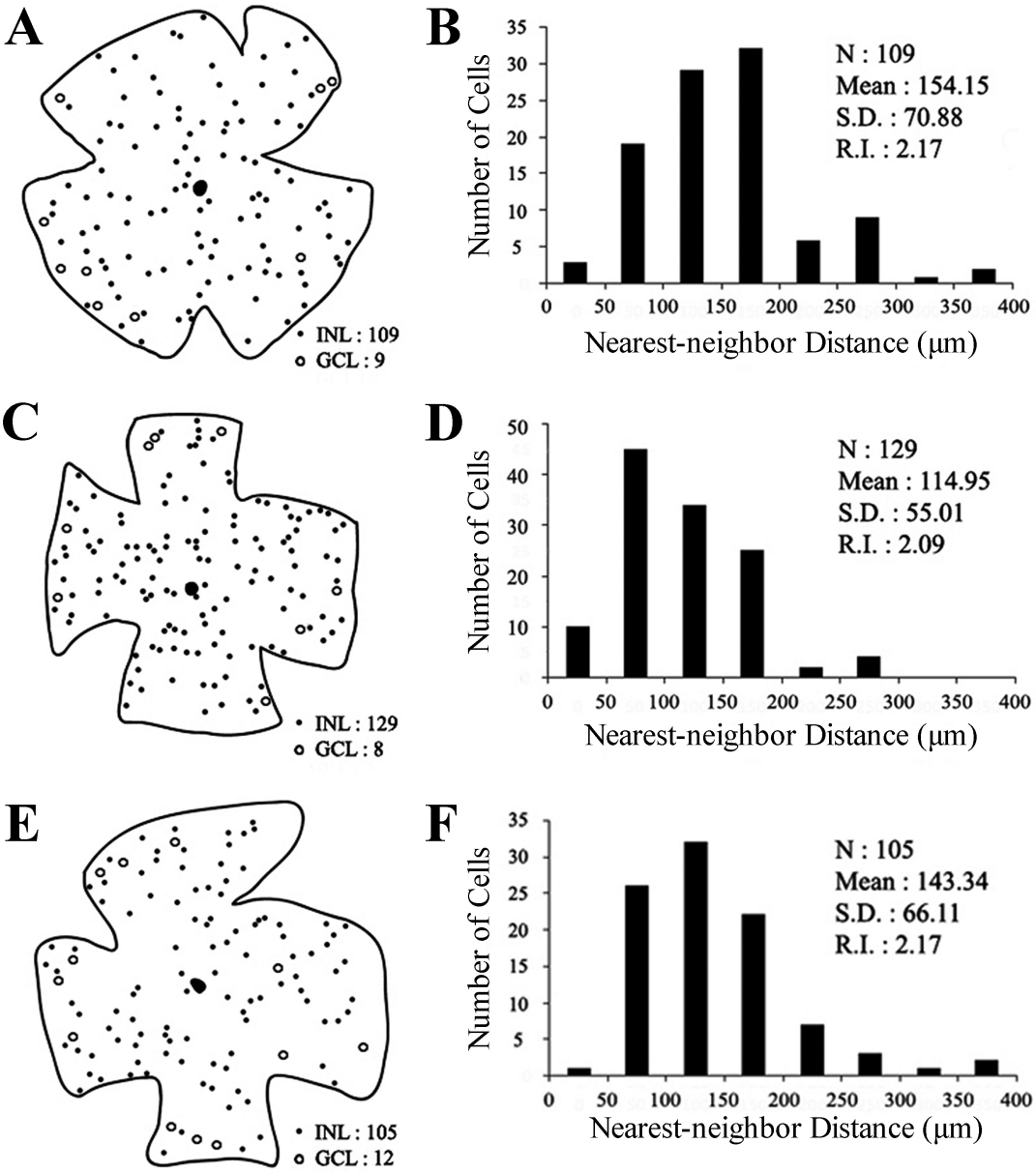

Fig. 6. Distribution and nearest-neighbor analysis of TH-IR cells in the *R. ferrumequinum* retina. **A, C, E.** Retinal distribution maps of total TH-IR cells. TH-IR cells in the INL are marked as dots and those in the GCL are marked as small circles. These respectively show the distributions of TH-IR cells measured for each nearest-neighbor analysis in **(B), (D),** and **(F)**. **B, D, F.** Histograms of TH-IR cells in the INL of three whole mount retinas showing the number of cells in the sample (N), mean distance between cells (Mean), standard deviation (S.D.), and the regularity index (R.I.). TH-IR cells in the GCL were exempt from this analysis. INL, inner nuclear layer; GCL, ganglion cell layer; N, number of cells; Mean, mean distance between cells; S.D., standard deviation; R.I., regularity index.

et al., 2000; Müller et al., 2013; Butz et al., 2015). In some primate retinas, other types of bipolar cells can also be labeled with PKCα. These include blue cone bipolar cells in human retina (Kolb et al., 1993) and ON diffuse (DB4) bipolar cells in monkey and human retina (Grünert et al., 1994; Haverkamp et al., 2003). However, in the present study, all PKCα-IR cells detected in the microbat *R. ferrumequinum* retina presented the typical morphology of rod bipolar cells observed in other mammals, with somata in the outer INL, dendritic processes in the OPL, and processes within the IPL with their varicose axon terminals extending to the lower IPL (McGuire et al., 1984; Greferath et al., 1990; Zhang and Yeh, 1991; Strettoi and Masland, 1995; Casini et al., 1996; Caminos et al., 2000). Consistent with our findings in the *R. ferrumequinum* retina, PKCα-IR cells in the retina of other microbats, *Carollia perspicillata* and *Glossophaga soricina*, also exhibit the typical morphology of rod bipolar cells (Müller et al., 2013). Therefore, the anti-PKCα antibody is a good marker for rod bipolar cells of the microbat retina. Characteristic axonal swellings were also visible in the middle IPL (S3) of the microbat *R. ferrumequinum* retina. Microbats *C. perspicillata* and *G. soricina* have layers of axonal swellings of PKCα-IR cells in S2 and S4 plus S5 of the IPL, where dendritic stratification of AII amacrine cells is present (Müller et al., 2013). In the *R. ferrumequinum* retina, AII amacrine cells extend their arboreal dendrites to the lower IPL and lobular appendages in the outer IPL, but not in the middle IPL (Jeon et al., 2007). Therefore, in the *R. ferrumequinum* retina, axonal swellings in the middle IPL might enhance the connections with other retinal neurons whose dendrites are stratified in the middle IPL. The unusual second axonal stratum of PKCα-IR cells seems to be one of the peculiarities of the microbat retina to strengthen their visual pathway.

Distribution of PKCα-IR cells in R. ferrumequinum retina

In the present study, the mean density of PKCα-IR cells in the *R. ferrumequinum* retina was 10,487±441 cells/mm^2 and the highest density was 14,900 cells/mm^2. The highest density of PKCα-IR cells varies between mammalian species (Table 3). The microbat retina has a relatively low number of rod bipolar cells compared with other mammalian retinas, except for the rabbit. The density distribution of PKCα-IR cells showed a regional

Table 3. Protein kinase C alpha immunoreactivity in various vertebrates from previous studies.

Species	References	Cell location	Axonal stratification within the IPL	Highest density (cells/mm^2)	Density distribution
Rabbit	Strettoi and Masland, 1995			5,450	highest density was found in the visual streak (3-4 mm away from optic nerve head)
	Young and Vaney, 1991	scleral portion of the INL	axons project to vitreal border of the IPL	5,000-7,000	
	Greferath et al., 1990	outer and middle INL	axon terminates in the inner IPL		
Cat	Greferath et al., 1990	middle to the outer INL	axons end very close to the GCL	46,000	highest density in the central temporal region, and decrease towards peripheral retina
Monkey	Grünert and Martin, 1991	frequently in the middle INL	two bands at the middle IPL (45-60%) and at the border with the GCL (80-105%)	19,000	dorsal region of the retina
	Grünert et al., 1994		axon terminals below the center of the IPL and close to GCL	13,000	increases from the central retina to the highest density, and then gradually decreases towards the peripheral region
Human	Haverkamp et al., 2003	middle to the outer INL	axons terminate in the inner IPL, close to the GCL		
Rat	Euler and Wässle, 1995	outermost INL, occasionally in the middle INL	axons to the inner border of the IPL	29,000 (mean: 20,000)	concentrated in the central temporal region
	Caminos et al., 2000	2-3 rows in the middle INL	some axon terminals reach the GCL	-	highest density of PKCα-IR cells was found in the peripheral region
Chicken	Caminos et al., 2000	a single row	axon terminals never reach the GCL	-	increases from the central retina to the highest density, and then gradually decreases towards the peripheral region
Goldfish, tench	Caminos et al., 2000	a single row in middle/outer INL	axon terminals never reach the GCL	-	increases from the central retina to the highest density in the peripheral region
Zebrafish	Caminos et al., 2000	2-3 rows in the middle INL	axon terminals never reach the GCL	-	increases from the central retina to the highest density in the peripheral region
Microbats *C. perspicillata* and *G. soricina*	Müller et al., 2013	outer half of the INL	two layers in S2 and S4 plus S5 of the IPL	-	-

IPL, inner plexiform layer; INL, inner nuclear layer; GCL, ganglion cell layer; S, sublamina.

difference in the *R. ferrumequinum* retina, with the highest density in the mid-central retina and the lowest density in the peripheral retina. Previous studies on PKCα-IR cells reported regional differences in cell density distribution throughout the whole retina, but with variations among different species (Table 3). For instance, in chicken retina (Caminos et al., 2000) and monkey retina (Grünert et al., 1994), the density of PKCα-IR cells increases from the central retina to the highest density, and then gradually decreases towards the peripheral region. However, the highest density of PKCα-IR cells was found in the peripheral region of goldfish, tench, zebrafish, and rat retinas (Caminos et al., 2000). Asymmetrical distribution pattern of PKCα-IR cell densities found in this study - the highest density in the nasal retina - can also be found in other mammalian retinas (see Table 3; Greferath et al., 1990; Grünert and Martin, 1991; Young and Vaney, 1991; Strettoi and Masland, 1995; Euler and Wässle, 1995). Therefore, there are species differences in the topographical distribution pattern of PKCα-IR cells over the retina.

Distributional comparison of PKCα-IR cells with rod photoreceptors and AII amacrine cells in R. ferrumequinum retina

The aforementioned distributional differences of PKCα-IR cells seem to be related to the distribution of other retinal neurons, particularly rod photoreceptors. The density distribution of rod bipolar cells was previously shown to match that of rod photoreceptors in various mammalian retinas (Young and Vaney, 1991; Grünert et al., 1994). While the overall distribution of rod photoreceptors is relatively flattened, the density of rod bipolar cells decreases rapidly with increasing eccentricity in the cat, monkey, and bat retinas (Greferath et al., 1990; Grünert and Martin, 1991; Kim et al., 2008), with variations in the ratio of rod photoreceptors to rod bipolar cells over the retina. This ratio has been analyzed in various mammalian retinas to identify the convergence of rod photoreceptors onto rod bipolar cells. The ratio differs between species. For instance, in the monkey retina, the ratio of rod photoreceptors to rod bipolar cells is approximately 12.5:1, increasing from a minimum of 5:1 to nearly 30:1 (Grünert and Martin, 1991; Grünert et al., 1994). In the cat retina, the ratio of rod photoreceptors to rod bipolar cells increases from 16:1 in the central region to 25:1 in the peripheral region (Greferath et al., 1990). The rabbit retina shows a ratio of approximately 50:1, increasing from 43:1 in the superior region to 58:1 in the inferior region (Young and Vaney, 1991; Strettoi and Masland, 1995). Our previous study conducted in the *R. ferrumequinum* retina (Kim et al., 2008) confirmed that microbats have a strongly rod-dominated retina with approximately 97.5% of the photoreceptors being rod cells. The collective prior and present data indicate that the overall distribution of rod photoreceptors and PKCα-IR rod bipolar cells is similar in the bat retina, and that the ratio of rod photoreceptors to rod bipolar cells is approximately 35:1, increasing from a minimum of 27:1 in the mid-central region to nearly 42:1 in the peripheral region. Therefore, it appears that many rod photoreceptors converge upon a single rod bipolar cell in the bat retina. The *R. ferrumequinum* retina has a relatively low number of rod bipolar cells compared to the number of rod photoreceptors in other species. However, microbats still have a higher density of rod bipolar cells in the retina and a lower ratio of rod photoreceptors to rod bipolar cells than the rabbit, which was reported to have a rod-dominated retina that is relatively poor in rod bipolar cells (Strettoi and Masland, 1995).

In the rod pathways of cats and rats, rod bipolar cells make glutamatergic synapses with AII amacrine cells, which in turn form synapses on the dendrites of ganglion cells and contribute rod signals to the ON and OFF pathways via their dendrites, which extend in both the ON and OFF sublaminae of the IPL (Kolb and Famiglietti, 1974; Famiglietti and Kolb, 1975; McGuire et al., 1984; Chun et al., 1993). The overall distribution of AII amacrine cells in the microbat *R. ferrumequinum* retina (Jeon et al., 2007) also displayed the highest density in the mid-central region and lowest density towards the peripheral region of the retina, although there were some regional differences in the highest and lowest density distributions. Therefore, the distribution of rod bipolar cells seems to be well correlated with the distribution of their input neurons (rod photoreceptors) and output neurons (AII amacrine cells). Along with previous quantitative analysis of rod photoreceptors (Kim et al., 2008) and AII amacrine cells (Jeon et al., 2007), the present study supports the presence of an anatomically well-organized visual network, including rod pathways, in the microbat *R. ferrumequinum* retina. Further physiological studies are needed for confirmation.

Types of TH-IR cells in R. ferrumequinum and other mammalian retinas

In the present study, four types of TH-IR cells were observed in *R. ferrumequinum* retinas: conventional amacrine, displaced amacrine, interplexiform, and intercalated cells. The majority of TH-IR cells were conventional amacrine cells. In other mammalian species, TH-IR cells are generally divided into one to three types (Table 4). Most mammalian retinas have three types of TH-IR cells: conventional amacrine, displaced amacrine, and interplexiform cells (Versaux-Botteri et al., 1984, 1986; Oyster et al., 1985; Eglen et al., 2003). In the rat retina (Versaux-Botteri et al., 1986), TH-IR catecholaminergic cells, which are not dopaminergic cells, were morphologically distinguished from TH-IR dopaminergic cells. The catecholaminergic cells have faintly-IR smaller soma with their processes stratified in the middle IPL and have been suggested to contribute to the visual processing of motion detection

(Versaux-Botteri et al., 1986; Knop et al., 2011; Brüggen et al., 2015). However, in the present study, TH-IR cells did not have morphological characteristics of those catecholaminergic cells. Moreover, even intercalated TH-IR cells had the same soma size with the conventional amacrine cells and showed strong immunoreactivity. Therefore, in bats, TH-IR cells might function as a dopaminergic neuron in the visual pathways. These variations in TH-IR cell types between species might indicate functional differences of the TH-IR cells in various species.

While most TH-IR processes are monostratified within the outermost IPL in mammalian retinas (Rodieck, 1998; Jeon et al., 2001), microbat TH-IR processes in the present study mainly branched to the outermost IPL, and additional processes branched to the middle (40%) or only sparsely to the innermost IPL (10%). Moreover, intercalated TH-IR cells within the IPL were rarely observed in the *R. ferrumequinum* retina with processes extending in the middle IPL. Taken together with a previous study in other microbat species (Studholme et al., 1987), the data suggest that TH immunoreactivity patterns differ even between the bat species (Table 4), implying that TH-IR dopaminergic amacrine cells may have slightly different roles among bat species, depending on their ecological characteristics. In most retinas, TH-IR dopaminergic amacrine cells are thought to communicate laterally by spreading their processes widely in a mostly monostratified manner in the outermost IPL. Therefore,

Table 4. Tyrosine hydroxylase immunoreactivity in various vertebrates from previous studies.

Species	References	Cell types	Stratification within the IPL	Mean density (cells/mm^2)	Distribution
Rabbit	Brecha et al., 1984	conventional amacrine cells located only in the proximal INL	mainly S1, other processes sparsely to S3 and 5, often discontinuous	19.4	nonrandom distribution (neither a random nor a regular); highest density in the visual streak (3 mm away from the prominent retinal blood vessels)
Bufo marinus	Zhu and Straznicky, 1990	conventional amacrine and displaced amacrine cells	mostly bistratification; prominent continuous plexus in scleral (S1), much sparser plexus in vitreal (S5)	36.6	orderly distribution; uneven distribution, non-uniform distribution; highest density in the temporo-central retina
Frog	Kicliter et al., 1999	conventional amacrine and displaced amacrine cells	bistratification; extensively to S1 and sparsely to S5	45	regular distribution; evenly distributed
Chicken	Teakle et al., 1993	conventional amacrine and displaced amacrine cells	S1 of the IPL, sparsely in S3, and short spiny dendrites at border of S4/S5	9.7	regular distribution; uneven distribution; highest density in central retina
Mouse	Versaux-Botteri et al., 1984	conventional amacrine, displaced amacrine, and interplexiform cells	mostly in the outermost sublayer of the IPL (S1)		random distribution; evenly distributed
Cat	Oyster et al., 1985	conventional amacrine, displaced amacrine, and interplexiform cells	most distal IPL adjacent to the INL, other processes in the proximal IPL		- ; uneven distribution
	Mitrofanis et al., 1988			9	
Rat	Versaux-Botteri et al., 1986	dopaminergic cells (with subtypes of displaced amacrine and interplexiform cells), catecholaminergic cells		24	uneven distribution; highest density in the upper temporal quadrant
Dog	Peichl, 1991	conventional amacrine, displaced amacrine, and interplexiform cells	mainly at the IPL/INL border, additional processes closer to the GCL	21.4	- ; uneven distribution
Ferret	Eglen et al., 2003	conventional amacrine, displaced amacrine, and interplexiform cells	monostratification (S1)	22.8	regular distribution; evenly distributed
Monkey	Guimarães and Hokoç, 1997	conventional amacrine, displaced amacrine, and interplexiform cells	arborization at three layers of the IPL, S1,3,5		- ; uneven distribution; highest density at 1-2 mm away from the central region
Macrotus waterhousii	Studholme et al., 1987	conventional amacrine cells	bistratified at distal border of IPL and distal third of IPL	-	-
Artibeus jamaicensis		conventional amacrine cells (and fibers in OPL)	monostratified at the distal border of the IPL (S1)	-	-
Glossophaga soricina and Monophyllus redmani		conventional and interstitial amacrine cells	bistratified at distal border of IPL and distal third of IPL	-	-

IPL, inner plexiform layer; INL, inner nuclear layer; GCL, ganglion cell layer; S, sublamina.

TH-IR dopaminergic amacrine cells with bistratified or multistratified processes in the microbat retina might facilitate more lateral and deeper communications in the IPL than those with monostratified processes in other species. It is difficult to assess how these morphological differences can affect functionality. However, since dopamine signaling is known to play critical roles in the mammalian retina by regulating circadian rhythms and light adaptation-induced changes (Balasubramanian and Gan, 2014), these morphological differences may be attributed to dark living environments, which need an amplification or modulation of dopamine signals to effectively manage circadian rhythms.

Distribution of TH-IR cells in R. ferrumequinum retina

In the *R. ferrumequinum retina*, most TH-IR cells were observed to be distributed in the INL, with a few TH-IR cells observed in the GCL. The mean densities of TH-IR cells in the INL and GCL were 27 cells/mm^2 and 2 cells/mm^2, respectively, with a total mean density of 30 cells/mm^2. The mean densities of TH-IR cells were as low as in other species (Table 4). Given the similar range of mean densities of total TH-IR cells in the retina among different species, this low density can be viewed as a common feature of TH-IR cells. The bat retina possesses this common characteristic despite slight differences in cell types and process ramification.

A retinal map and nearest-neighbor analysis were used to elucidate the spatial distribution of TH-IR cells. Based on the calculated regularity index (2.14±0.05, n=3; Cook, 1996), we can conclude that TH-IR cells of the INL are distributed nonrandomly over the *R. ferrumequinum* retina. In most other species, such as frogs (Kicliter et al., 1999), *Bufo marinus* (Zhu and Straznicky, 1990), turtles (Kolb et al., 1987), ferrets (Eglen et al., 2003), and rabbits (Brecha et al., 1984), there is a nonrandom distribution of TH-IR cells in the INL of the retina. There are variations among species in the regularity of the TH-IR cell distribution and the density distribution (even or uneven pattern) of the TH-IR cells (Table 4). Retinal TH-IR cells in many mammals are not evenly distributed, and the density distribution patterns vary markedly depending on the species. However, some vertebrates, such as turtles (Kolb et al., 1987), frogs (Kicliter et al., 1999), and ferrets (Eglen et al., 2003), have an even density distribution. These differences suggest that there may be functional relationships between dopaminergic amacrine cells and other retinal neurons. In the monkey retina, the density distribution pattern of TH-IR cells was correlated with that of photoreceptors (Mariani et al., 1984), suggesting that TH-IR cells are closely related to rod systems. In rabbit and rat retina, ganglion cell distribution seems to correlate with TH-IR amacrine cells (Brecha et al., 1984; Versaux-Botteri et al., 1986). Since the distribution of rod photoreceptors in the *R. ferrumequinum* retina (Kim et al., 2008) shows a flat distribution similar to TH-IR cells, we can also suggest that TH-IR cells in the *R. ferrumequinum* retina might be closely related to rod pathways.

Connections of TH-IR cells with AII amacrine cells in R. ferrumequinum retina

We observed that TH-IR processes in the *R. ferrumequinum* retina formed ring-like structures around the somata of AII amacrine cells. This is similar to dopaminergic cells of other mammalian retinas (Törk and Stone, 1979; Pourcho, 1982; Oyster et al., 1985; Voigt and Wässle, 1987; Dacey, 1990; Kolb et al., 1990, 1991; Völgyi et al., 2014; Debertin et al., 2015). This might indicate that AII amacrine cells are the main target of dopamine signaling via TH-IR neurons, which enables the modulatory effects on scotopic vision and retinal sensitivity during light and dark adaptation (Piccolino et al., 1987; Voigt and Wässle, 1987; Gustincich et al., 1997; Feigenspan et al., 1998; Zhang et al., 2008). Thus, our results could support the view that microbat retinas can successfully respond to light or dark stimulation. Since some ring-like structures encircle non-AII amacrine cells, dopamine secretion of TH-IR cells in the *R. ferrumequinum* retina may affect the sensitivity of different retinal neurons. Therefore, our overall data suggest that TH-IR cells with wide-spread networks across the *R. ferrumequinum* retina play significant roles in controlling the sensitivities of many retinal neurons. These results reinforce the notion that *R. ferrumequinum* retina has well-connected neuronal circuits that provide functional visual processing.

In conclusion, microbats may have an anatomically organized visual network and functional modulatory mechanisms for scotopic vision via rod bipolar cells and dopaminergic neurons. Stratification differences of TH-IR cells possibly reflect the requirements on the visual system of microbats through their nocturnal lifestyle. This supports the previous suggestions and reports that microbat eyes have not atrophied, but rather have systematic roles in visual function (Müller et al., 2009; Orbach and Fenton, 2010; Müller et al., 2013; Butz et al., 2015; Park et al., 2017). Future studies on visual systems and their connections to the brain using the present study as the foundation may reinforce the view that the visual pathways of microbats can perform visual processing functions and are not atrophied.

*Acknowledgements.*We thank Cactus Communications for proofreading the manuscript. This research was supported by the Basic Science Research Program through the National Research Foundation of Korea (NRF), funded by the Ministry of Education (NRF-2016R1D1A1A09918427).

References

Altringham J.D. (2011). Bats: From evolution to conservation. 2nd ed. Oxford University Press. New York.

Baden T., Berens P., Franke K., Rosón M.R., Bethge M. and Euler T.

(2016). The functional diversity of retinal ganglion cells in the mouse. Nature 529, 345-350.

Balasubramanian R. and Gan L. (2014). Development of retinal amacrine cells and their dendritic stratification. Curr. Ophthalmol. Rep. 2, 100-106.

Brecha N.C., Oyster C.W. and Takahashi E.S. (1984). Identification and characterization of tyrosine hydroxylase immunoreactive amacrine cells. Invest. Ophthalmol. Vis. Sci. 25, 66-70.

Brüggen B., Meyer A., Boven F., Weiler R. and Dedek K. (2015). Type 2 wide-field amacrine cells in TH::GFP mice show a homogenous synapse distribution and contact small ganglion cells. Eur. J. Neurosci. 41, 734-747.

Butz E., Peichl L. and Müller B. (2015). Cone bipolar cells in the retina of the microbat Carollia perspicillata. J. Comp. Neurol. 523, 963-981.

Caminos E., Velasco A., Jarrín M., Lillo C., Jimeno D., Aijón J. and Lara J.M. (2000). A comparative study of protein kinase C-like immunoreactive cells in the retina. Brain Behav. Evol. 56, 330-339.

Casini G., Grassi A., Trasarti L. and Bagnoli P. (1996). Developmental expression of protein kinase C immunoreactivity in rod bipolar cells of the rabbit retina. Vis. Neurosci. 13, 817-831.

Casini G., Rickman D.W. and Brecha N.C. (1995). AII amacrine cell population in the rabbit retina: Identification by parvalbumin immunoreactivity. J. Comp. Neurol. 356, 132-142.

Chun M.H., Han S.H., Chung J.W. and Wässle H. (1993). Electron microscopic analysis of the rod pathway of the rat retina. J. Comp. Neurol. 332, 421-432.

Conn P.J. and Sweatt J.D. (1994). Protein kinase C in the nervous system. Oxford University Press. New York.

Cook J.E. (1996). Spatial properties of retinal mosaics: An empirical evaluation of some existing measures. Vis. Neurosci. 13, 15-30.

Dacey D.M. (1990). The dopaminergic amacrine cell. J. Comp. Neurol. 301, 461-489.

Debertin G., Kántor O., Kovács-Öller T., Balogh L., Szabó-Meleg E., Orbán J., Nyitrai M. and Völgyi B. (2015). Tyrosine hydroxylase positive perisomatic rings are formed around various amacrine cell types in the mammalian retina. J. Neurochem. 134, 416-428.

Dowling J.E. (1987). The retina: An approachable part of the brain. Harvard University Press. Massachusetts and London.

Eglen S.J., Raven M.A., Tamrazian E. and Reese B.E. (2003). Dopaminergic amacrine cells in the inner nuclear layer and ganglion cell layer comprise a single functional retinal mosaic. J. Comp. Neurol. 466, 343-355.

Eklöf J. (2003). Vision in echolocating bats. Doctoral thesis. Göteborg University. Göteborg.

Euler T. and Wässle H. (1995). Immunocytochemical identification of cone bipolar cells in the rat retina. J. Comp. Neurol. 361, 461-478.

Euler T., Haverkamp S., Schubert T. and Baden T. (2014). Retinal bipolar cells: Elementary building blocks of vision. Nat. Rev. Neurosci. 15, 507-519.

Famiglietti E.V.J. and Kolb H. (1975). A bistratified amacrine cell and synaptic circuitry in the inner plexiform layer of the retina. Brain Res. 84, 293-300.

Feigenspan A., Gustincich S., Bean B.P. and Raviola E. (1998). Spontaneous activity of solitary dopaminergic cells of the retina. J. Neurosci. 18, 6776-6789.

Feller K.D., Lagerholm S., Clubwala R., Silver M.T., Haughey D., Ryan J.M., Loew E.R., Deutschlander M.E. and Kenyon K.L. (2009). Characterization of photoreceptor cell types in the little brown bat *Myotis Lucifugus* (Vespertilionidae). Comp. Biochem. Physiol. B Biochem. Mol. Biol. 154, 412-418.

Gábriel R. and Straznicky C. (1992). Immunocytochemical localization of parvalbumin- and neurofilament triplet protein immunoreactivity in the cat retina: Colocalization in a subpopulation of AII amacrine cells. Brain Res. 595, 133-136.

Greferath U., Grünert U. and Wässle H. (1990). Rod bipolar cells in the mammalian retina show protein kinase C-like immunoreactivity. J. Comp. Neurol. 301, 433-442.

Grünert U. and Martin P.R. (1991). Rod bipolar cells in the macaque monkey retina: Immunoreactivity and connectivity. J. Neurosci. 11, 2742-2758.

Grünert U., Martin P.R. and Wässle H. (1994). Immunocytochemical analysis of bipolar cells in the macaque monkey retina. J. Comp. Neurol. 348, 607-627.

Guimarães P.Z. and Hokoç J.N. (1997). Tyrosine hydroxylase expression in the Cebus monkey retina. Vis. Neurosci. 14, 705-715.

Gustincich S., Feigenspan A., Wu D.K., Koopman L.J. and Raviola E. (1997). Control of dopamine release in the retina: A transgenic approach to neural networks. Neuron 18, 723-736.

Haverkamp S., Haeseleer F. and Hendrickson A. (2003). A comparison of immunocytochemical markers to identify bipolar cell types in human and monkey retina. Vis. Neurosci. 20, 589-600.

Jeon M.H. and Jeon C.J. (1998). Immunocytochemical localization of calretinin containing neurons in retina from rabbit, cat, and dog. Neurosci. Res. 32, 75-84.

Jeon Y.K., Kim S.Y. and Jeon C.J. (2001). Morphology of calretinin and tyrosine hydroxylase-immunoreactive neurons in the pig retina. Mol. Cells 11, 250-256.

Jeon Y.K., Kim T.J., Lee J.Y., Choi J.S. and Jeon C.J. (2007). AII amacrine cells in the inner nuclear layer of bat retina: Identification by parvalbumin immunoreactivity. Neuroreport 18, 1095-1099.

Jones G. and Rayner J.M.V. (1989). Foraging behavior and echolocation of wild horseshoe bats *Rhinolophus ferrumequinum* and *R. hipposideros* (Chiroptera, Rhinolophidae). Behav. Ecol. Sociobiol. 25, 183-191.

Kicliter E., Bengoa F., Herrera J.A., González M., Ortíz-Goveo E., Rodríguez V. and Lugo N. (1999). Two groups of TH-like immunoreactive neurons in the frog (*Rana pipiens*) retina. Brain Res. 816, 149-157.

Kim T.J., Jeon Y.K., Lee J.Y., Lee E.S. and Jeon C.J. (2008). The photoreceptor populations in the retina of the greater horseshoe bat *Rhinolophus ferrumequinum*. Mol. Cells 26, 373-379.

Knop G.C., Feigenspan A., Weiler R. and Dedek K. (2011). Inputs underlying the ON-OFF light responses of type 2 wide-field amacrine cells in TH::GFP mice. J. Neurosci. 31, 4780-4791.

Kolb H. and Famiglietti E.V. (1974). Rod and cone pathways in the inner plexiform layer of cat retina. Science 186, 47-49.

Kolb H., Cline C., Wang H.H. and Brecha N. (1987). Distribution and morphology of dopaminergic amacrine cells in the retina of the turtle (*Pseudemys scripta elegans*). J. Neurocytol. 16, 577-588.

Kolb H., Cuenca N. and Dekorver L. (1991). Postembedding immunocytochemistry for GABA and glycine reveals the synaptic relationships of the dopaminergic amacrine cell of the cat retina. J. Comp. Neurol. 310, 267-284.

Kolb H., Cuenca N., Wang H.H. and Dekorver L. (1990). The synaptic organization of the dopaminergic amacrine cell in the cat retina. J. Neurocytol. 19, 343-366.

Kolb H., Zhang L. and Dekorver L. (1993). Differential staining of neurons in the human retina with antibodies to protein kinase C

isozymes. Vis. Neurosci. 10, 341-351.

Kosaka J., Suzuki A., Morii E. and Nomura S. (1998). Differential localization and expression of α and β isoenzymes of protein kinase C in the rat retina. J. Neurosci. Res. 54, 655-663.

Mariani A.P., Kolb H. and Nelson R. (1984). Dopamine-containing amacrine cells of rhesus monkey retina parallel rods in spatial distribution. Brain Res. 322, 1-7.

Masland R.H. (2004). Neuronal cell types. Curr. Biol. 14, R497-500.

McGuire B.A., Stevens J.K. and Sterling P. (1984). Microcircuitry of bipolar cells in cat retina. J. Neurosci. 4, 2920-2938.

Mitrofanis J., Vigny A. and Stone J. (1988). Distribution of catecholaminergic cells in the retina of the rat, guinea pig, cat, and rabbit: Independence from ganglion cell distribution. J. Comp. Neurol. 267, 1-14.

Müller B., Butz E., Peichl L. and Haverkamp S. (2013). The rod pathway of the microbat retina has bistratified rod bipolar cells and tristratified AII amacrine cells. J. Neurosci. 33, 1014-1023.

Müller B., Glösmann M., Peichl L., Knop G.C., Hagemann C. and Ammermüller J. (2009). Bat eyes have ultraviolet-sensitive cone photoreceptors. PLoS One 4, e6390.

Negishi K., Kato S. and Teranishi T. (1988). Dopamine cells and rod bipolar cells contain protein kinase C-like immunoreactivity in some vertebrate retinas. Neurosci. Lett. 94, 247-252.

Nishizuka Y. (1988). The molecular heterogeneity of protein kinase C and its implications for cellular regulation. Nature 334, 661-665.

Nishizuka Y. (1992). Intracellular signaling by hydrolysis of phospholipids and activation of protein kinase C. Science 258, 607-614.

Orbach D.N. and Fenton B. (2010). Vision impairs the abilities of bats to avoid colliding with stationary obstacles. PLoS One 5, e13912.

Oyster C.W., Takahashi E.S., Cilluffo M. and Brecha N.C. (1985). Morphology and distribution of tyrosine-hydroxylase-like immunoreactive neurons in the cat retina. Proc. Natl. Acad. Sci. USA 82, 6335-6339.

Park E.B., Gu Y.N. and Jeon C.J. (2017). Immunocytochemical localization of cholinergic amacrine cells in the bat retina. Acta Histochem. 119, 428-437.

Peichl L. (1991). Catecholaminergic amacrine cells in the dog and wolf retina. Vis. Neurosci. 7, 575-587.

Piccolino M., Witkovsky P. and Trimarchi C. (1987). Dopaminergic mechanisms underlying the reduction of electrical coupling between horizontal cells of the turtle retina induced by d-amphetamine, bicuculline, and veratridine. J. Neurosci. 7, 2273-2284.

Pourcho R.G. (1982). Dopaminergic amacrine cells in the cat retina. Brain Res. 252, 101-109.

Rodieck R.W. (1998). The first steps in seeing. Sinauer Associates. Massachusetts.

Sanes J.R. and Masland R.H. (2015). The types of retinal ganglion cells: Current status and implications for neuronal classification. Annu. Rev. Neurosci. 38, 221-246.

Strettoi E. and Masland R.H. (1995). The organization of the inner nuclear layer of the rabbit retina. J. Neurosci. 15, 875-888.

Studholme K.M., Yazulla S. and Phillips C.J. (1987). Interspecific comparisons of immunohistochemical localization of retinal neurotransmitters in four species of bats. Brain Behav. Evol. 30, 160-173.

Teakle E.M., Wildsoet C.F. and Vaney D.I. (1993). The spatial organization of tyrosine hydroxylase-immunoreactive amacrine cells in the chicken retina and the consequences of myopia. Vision Res. 33, 2383-2396.

Törk I. and Stone J. (1979). Morphology of catecholamine-containing amacrine cells in the cat's retina, as seen in retinal whole mounts. Brain Res. 169, 261-273.

Versaux-Botteri C., Martin-Martinelli E., Nguyen-Legros J., Geffard M., Vigny A. and Denoroy L. (1986). Regional specialization of the rat retina: Catecholamine-containing amacrine cell characterization and distribution. J. Comp. Neurol. 243, 422-433.

Versaux-Botteri C., Nguyen-Legros J., Vigny A. and Raoux N. (1984). Morphology, density and distribution of tyrosine hydroxylase-like immunoreactive cells in the retina of mice. Brain Res. 301, 192-197.

Voigt T. and Wässle H. (1987). Dopaminergic innervation of AII amacrine cells in mammalian retina. J. Neurosci. 7, 4115-4128.

Völgyi B., Debertin G., Balogh M., Popovich E. and Kovács-Öller T. (2014). Compartment-specific tyrosine hydroxylase-positive innervation to AII amacrine cells in the rabbit retina. Neuroscience 270, 88-97.

Wässle H. and Riemann H.J. (1978). The mosaic of nerve cells in the mammalian retina. Proc. R. Soc. Lond. B Biol. Sci. 200, 441-461.

Wässle H., Grünert U. and Röhrenbeck J. (1993). Immunocytochemical staining of AII-amacrine cells in the rat retina with antibodies against parvalbumin. J. Comp. Neurol. 332, 407-420.

Wässle H., Grünert U., Chun M.H. and Boycott B.B. (1995). The rod pathway of the macaque monkey retina: Identification of AII-amacrine cells with antibodies against calretinin. J. Comp. Neurol. 361, 537-551.

Winter Y., López J. and Von Helversen O. (2003). Ultraviolet vision in a bat. Nature 425, 612-614.

Young H.M. and Vaney D.I. (1991). Rod-signal interneurons in the rabbit retina: 1. Rod bipolar cells. J. Comp. Neurol. 310, 139-153.

Zhang D.R. and Yeh H.H. (1991). Protein kinase C-like immunoreactivity in rod bipolar cells of the rat retina: A developmental study. Vis. Neurosci. 6, 429-437.

Zhang D.Q., Wong K.Y., Sollars P.J., Berson D.M., Pickard G.E. and McMahon D.G. (2008). Intraretinal signaling by ganglion cell photoreceptors to dopaminergic amacrine neurons. Proc. Natl. Acad. Sci. USA 105, 14181-14186.

Zhu B. and Straznicky C. (1990). Dendritic morphology and retinal distribution of tyrosine hydroxylase-like immunoreactive amacrine cells in *Bufo marinus*. Anat. Embryol. 181, 365-371.

Accepted May 9, 2018